

7-19-2018

# Open Resonance Assisted Hydrogen Bonds and Competing Quasiaromaticity

Yen H. Nguyen

*Iowa State University*, yhnghuyen@iastate.edu

Bryan J. Lampkin

*Iowa State University*, blampkin@iastate.edu

Amrit Venkatesh

*Iowa State University*, amritv@iastate.edu

Arkady Ellern

*Iowa State University*, ellern@iastate.edu

Aaron J. Rossini

*Iowa State University*, arossini@iastate.edu

*See next page for additional authors*

Follow this and additional works at: [https://lib.dr.iastate.edu/chem\\_pubs](https://lib.dr.iastate.edu/chem_pubs)



Part of the [Organic Chemistry Commons](#)

The complete bibliographic information for this item can be found at [https://lib.dr.iastate.edu/chem\\_pubs/1036](https://lib.dr.iastate.edu/chem_pubs/1036). For information on how to cite this item, please visit <http://lib.dr.iastate.edu/howtocite.html>.

---

This Article is brought to you for free and open access by the Chemistry at Iowa State University Digital Repository. It has been accepted for inclusion in Chemistry Publications by an authorized administrator of Iowa State University Digital Repository. For more information, please contact [digirep@iastate.edu](mailto:digirep@iastate.edu).

---

# Open Resonance Assisted Hydrogen Bonds and Competing Quasiaromaticity

## Abstract

The delocalization of electron density upon tautomerization of a proton across a conjugated bridge can alter the strength of hydrogen bonds. This effect has been dubbed resonance-assisted hydrogen bonding (RAHB) and plays a major role in the energetics of the tautomeric equilibrium. The goal of this work was to investigate the role that  $\pi$ -delocalization plays in the stability of RAHBs by engaging other isomerization processes. Similarly, acid-base chemistry has received little experimental attention in studies of RAHB and we address the role that acid-base effects play in the tautomeric equilibrium. We find that  $\pi$ -delocalization and the disruption of adjacent aromatic rings is the dominant effect in determining the stability of a RAHB.

## Disciplines

Organic Chemistry

## Comments

This is a manuscript of an article published as Nguyen, Yen H., Bryan J. Lampkin, Amrit Venkatesh, Arkady Ellern, Aaron J. Rossini, and Brett VanVeller. "Open Resonance Assisted Hydrogen Bonds and Competing Quasiaromaticity." *The Journal of organic chemistry* (2018). Posted with permission.

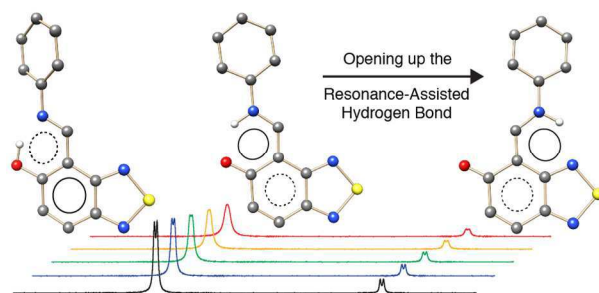
## Authors

Yen H. Nguyen, Bryan J. Lampkin, Amrit Venkatesh, Arkady Ellern, Aaron J. Rossini, and Brett VanVeller

# Open Resonance Assisted Hydrogen Bonds and Competing Quasiaromaticity

Yen H. Nguyen, Bryan J. Lampkin, Amrit Venkatesh, Arkady Ellern, Aaron J. Rossini, and Brett VanVeller\*

Department of Chemistry, Iowa State University, Ames, Iowa 50011, United States



## ABSTRACT

The delocalization of electron density upon tautomerization of a proton across a conjugated bridge can alter the strength of hydrogen bonds. This effect has been dubbed resonance-assisted hydrogen bonding (RAHB) and plays a major role in the energetics of the tautomeric equilibrium. The goal of this work was to investigate the role that  $\pi$ -delocalization plays in the stability of RAHBs by engaging other isomerization processes. Similarly, acid-base chemistry has received little experimental attention in studies of RAHB and we address the role that acid-base effects play in the tautomeric equilibrium. We find that  $\pi$ -delocalization and the disruption of adjacent aromatic rings is the dominant effect in determining the stability of a RAHB.

## INTRODUCTION

The tautomeric equilibrium between enolamines (OH-form) and enamines (NH-form, Figure 1A) plays a critical role in biosynthesis and medicinal chemistry.<sup>1</sup> For example, the Schiff bases of pyridoxal phosphate (Figure 1B) are important in the enzymatic transformations of amino acids, where proton transfer between oxygen and nitrogen is often the first step of the catalytic cycle.<sup>2-4</sup> Additionally, several enolimine drugs have been reported that act on the central nervous system<sup>5,6</sup> and  $K^+$  channels.<sup>7</sup> Similarly, sirtinol (Fig 1B) is a deacetylase inhibitor<sup>8</sup> that displays anticancer<sup>9-14</sup> and antiviral<sup>15</sup> activity. The structure of sirtinol features a Schiff base with 2-hydroxynaphthalene, which is important for drug action.<sup>8,16</sup>

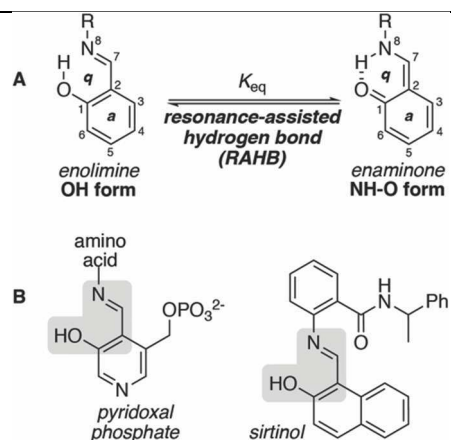
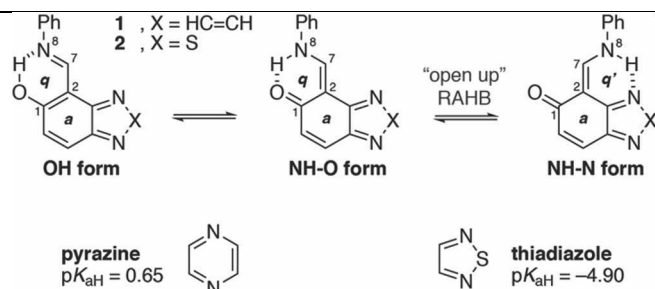


**Figure 1.** **A**, tautomeric equilibrium of enolimine and enaminone. **B**, tautomeric examples.

The balance of the equilibrium between both tautomeric forms is partially dependent on the  $\pi$ -delocalization in both of the rings indicated in Figure 1A (**a** and **q**).<sup>17-22</sup> The  $\pi$ -delocalization in ring **q** favors the enaminone (NH-O) tautomer with a strong O $\cdots$ H hydrogen bond<sup>23,24</sup> and this stabilization is termed a resonance-assisted hydrogen bond (RAHB).<sup>1,21,23-27</sup> While the tautomeric equilibrium can be affected by substituents,<sup>1,28</sup> in general, an increase in the aromaticity of ring **q** leads to a loss of aromaticity in ring **a**,<sup>1,16,21,29,30</sup> and these results suggest that  $\pi$ -delocalization in ring **a** and **q** are coupled to each other. This interplay was recently demonstrated to operate in the excited state as well.<sup>31</sup> To investigate the coupling of  $\pi$ -delocalization further, we sought to “open up” the RAHB to engage a new tautomeric, quasiaromatic structure (Scheme 1). Previous studies have sought to entice the proton in Figure 1A away from the traditional RAHB but have not been successful.<sup>16</sup>



**Scheme 1.** Tautomeric forms under consideration

Intriguingly, the RAHB equilibrium of Figure 1A has not received much attention in the context of heterocycles. Most experimental studies have focused on all-carbon cycles except for some reports that employ the pyridine or quinolone nitrogen in the role of the Schiff-base in Figure 1A.<sup>32-34</sup> We hypothesized that nitrogen heterocycles could suitably position Lewis basic atoms to coax the **NH-O** form to open up to an unprecedented **NH-N** form (Scheme 1). To test our hypothesis, we elected to focus on **1** and **2** (Scheme 1 and 2) for three reasons: (i) The geometry of the RAHB in ring *q'* is different for both compounds. The 6-membered pyrazine ring in **1** presents a different hydrogen bonding geometry than the thiadiazole ring in **2**. This geometric effect might alter the stability of the RAHB in *q'*. (ii) The basicity of the nitrogen atoms in each compound are different. The large difference in the  $pK_{aH}$  values of the parent heterocycles, pyrazine and thiadiazole (Scheme 1), may also play a role in enticing the **NH-O** form to open up into the **NH-N** form. (iii) It has been proposed that  $\pi$ -delocalization within the RAHB heavily perturbs the OH  $pK_a$ , ultimately making analysis of the effect of acidity difficult<sup>35</sup> or impossible.<sup>28</sup> For this reason, we sought to clarify our analysis and control for OH acidity by employing compounds with similar "initial"  $pK_a$  values at the OH group. Towards this goal, we selected quinoxaline (**3**) and benzothiadiazole (**4**) because we measured similar OH  $pK_a$  values for both compounds (Figure 2). The similar acidities of these base heterocycles also imply similar electron-withdrawing effects in both compounds.

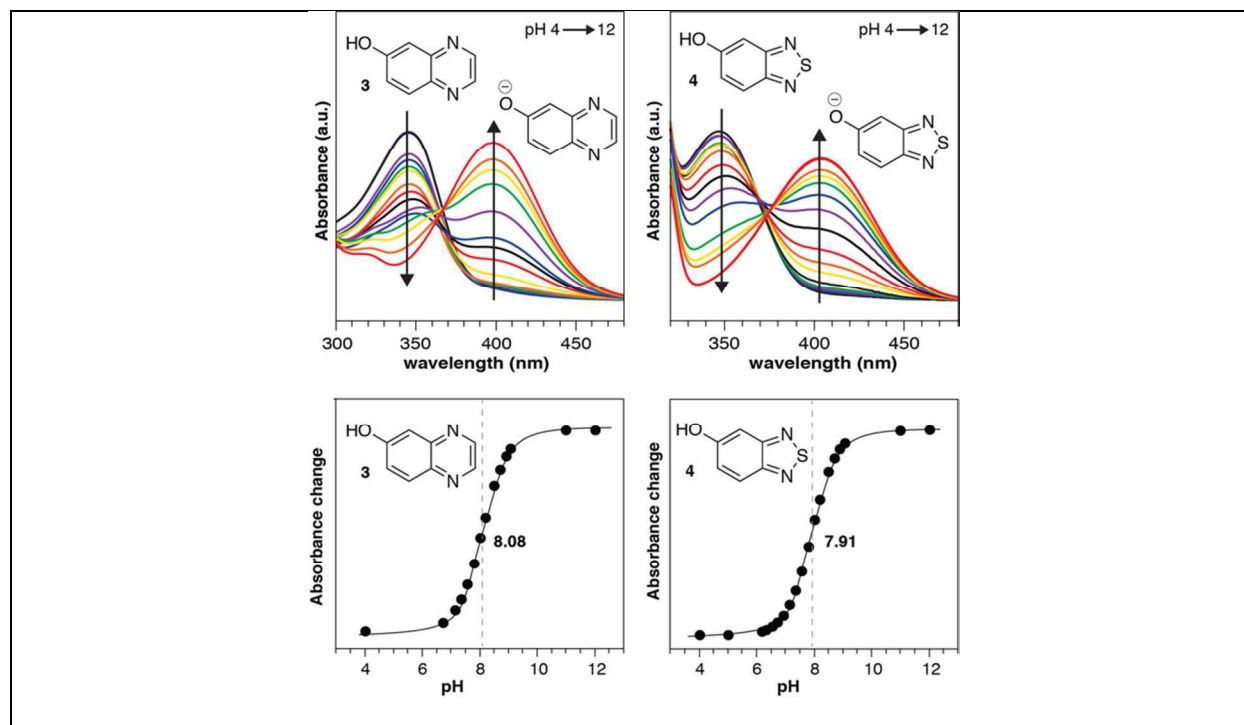
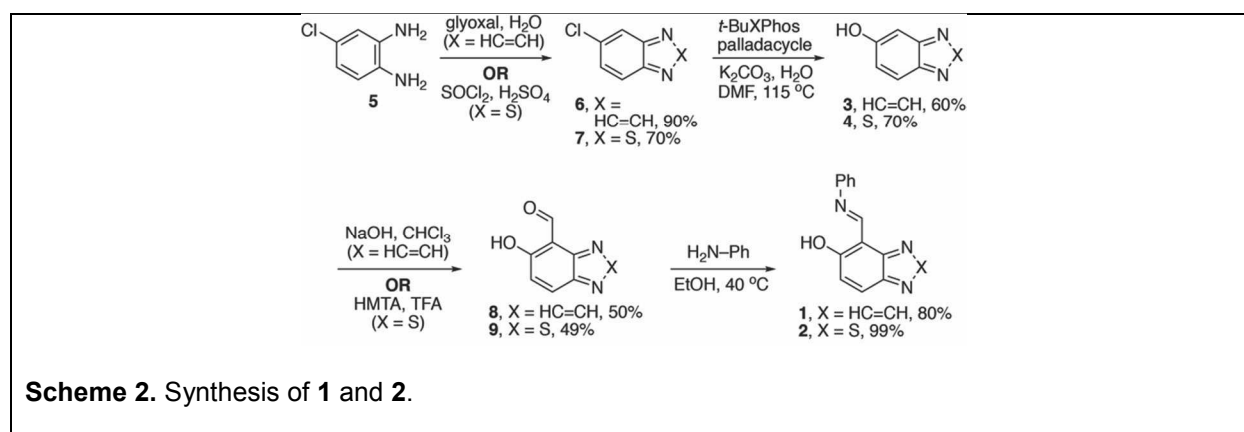


**Figure 2.** Determination of  $pK_a$  of compounds **3** and **4** by monitoring the onset of phenolate formation.<sup>36</sup> See SI for experimental details and data processing.

## RESULTS AND DISCUSSION

The synthesis of **1** and **2** commenced with diamine **5** as the starting point for both molecules. Closure of the pyrazine ring to form **6** was achieved via condensation with glyoxal,<sup>37</sup> while the benzothiadiazole variant (**7**) was synthesized using thionyl chloride in sulfuric acid.<sup>38</sup> Substitution of  $-Cl$  for  $-OH$  was performed via Pd-catalyzed cross coupling to give **3** and **4**.<sup>39</sup> Installation of the aldehyde required two distinct conditions for each heterocycle. The Reimer–Tiemann reaction was required to convert **3** to **8**,<sup>40</sup> while the Duff reaction<sup>41</sup> using hexamethylenetetramine (HMTA)<sup>42</sup> was employed to convert **4** to **9**.<sup>42</sup> The final Schiff bases were readily accessed upon condensation with aniline in ethanol to give **1** and **2**.



Examination of the NMR data of **1** and **2** provided insight into the dynamic tautomeric equilibrium proposed in Scheme 1 and reveals that the unprecedented **NH-N** form was present in both compounds. Various NMR solvents were used for the characterization of compounds **3–9**, and assigned NMR spectra for **1** and **2** in  $CDCl_3$  used for analysis can be found in the SI (pages S3-S4).

### A. Evidence of only two forms in solution

The **OH** and **NH-O** forms cannot be distinguished spectroscopically because proton exchange is fast on the NMR time-scale. Thus, a single peak is observed for the **OH/NH-O** ensemble (Figure 3, Table 1). For both **1** and **2**, however, another form is observable in solution and corresponds to the **NH-N** form. Other tautomeric structures of **1** and **2** were disqualified because they were deemed to be too high in

energy to warrant consideration based on their calculated energies (Scheme 3, *vide infra* and Figure S20).

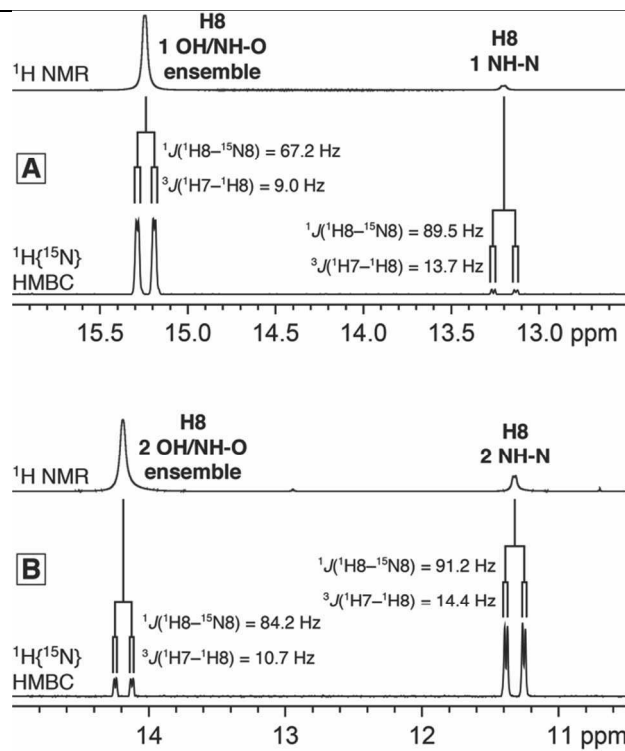


**Figure 3.** NMR data for (A) **1** and (B) **2**. One-dimensional  $^1\text{H}$  NMR (top) and  $^1\text{H}$  projections from the 2D  $^1\text{H}\{^{15}\text{N}\}$  HMBC experiments (bottom).

### B. Dominance of NH-O within the OH/NH-O ensemble

Both **1 OH/NH-O** and **2 OH/NH-O** exist predominantly (> 85%) in their **NH-O** forms, as evinced by the following data summarized in Table 1: (i) A  $^3J_{\text{HH}}$  splitting is observed between H7 and NH8 for both compounds (Figure 3, Table 1, row 1 and 2), indicating that the **NH-O** form dominates over the **OH** form. (ii) The chemical shift of C1 in both compounds (row 3) approaches a shift more similar to a carbonyl carbon (~190 ppm) than a phenolic carbon (~160 ppm). (iii) The chemical shift of  $^{15}\text{N8}$  (row 4) similarly indicates the dominance of the **NH-O** form. The observed  $^{15}\text{N}$  chemical shifts are typical of those for conjugated NH (ca. -200 ppm), while an imine nitrogen chemical shift typically occurs between -25 to -90 ppm.<sup>43</sup> Finally, Figure 4 displays the X-ray crystal structures of **1** and **2** with the position of H8 determined by dispersion-corrected plane-wave DFT calculations. Plane-wave DFT was used to take account of the periodicity of the crystal structure and more accurately locate the hydrogen atom within the

1  
2  
3 crystal structure. The experimentally measured C–C, C–N and C–O bond lengths correspond to those of  
4 the **NH-O** form and are consistent with the NH tautomer being the lower energy form in the crystal  
5 state,<sup>1,44</sup> likely due to the higher proton affinity of N versus O.<sup>29,45-48</sup> Previously reported crystal structures  
6 of Schiff-base RAHB compounds can show solid-state intermolecular interactions that directly contact the  
7 RAHB and cause the **OH** form to be lower in energy. In contrast to these previous reports,<sup>49,50</sup> however,  
8 there are no clear intermolecular interactions with the RAHB of **1** and **2** evident in the crystal states  
9 (Figure S15 and S16).

### 16 C. Evidence for the **NH-N** form

17  
18 Inspection of the  $^1\text{H}\{^{15}\text{N}\}$  HMBC NMR spectra reveals two distinct cross-peaks that reveal the  
19  $^1J_{\text{NH}}(^1\text{H8}-^{15}\text{N8})$  coupling (Figure 3). The major set of  $^1\text{H}$  NMR signals corresponds to the **NH-O** form and  
20 the second, minor set of signals are assigned to the **NH-N** form in both **1** and **2**. The ratio between the  
21 **OH/NH-O** ensemble and the **NH-N** form was measured directly from the proton signal integration and  
22 indicates that only 6% and 15% of **1** and **2** are found in the **NH-N** form, respectively (Table 1, row 5). It is  
23 noteworthy that the **NH-N** form opens up the classical RAHB in ring **q** to form an unprecedented, new  
24 quasiaromatic ring **q'**.<sup>16</sup> The tautomeric state of the **NH-N** form is similarly support by the spectroscopic  
25 evidence as for **NH-O** above (rows 1–4). Transfer of the proton to the nitrogen of the heterocycle (from  
26 N8-H to N3-H) was calculated to be too high in energy to be observable (Scheme 3). However, the  
27  $^1\text{H}\{^{15}\text{N}\}$  HMBC NMR show a weak correlation between H8 and N3 at lower temperatures of 273 K,  
28 consistent with the presence of a weak hydrogen bond (Figure S12).  
29  
30  
31  
32  
33  
34  
35  
36  
37  
38  
39  
40  
41  
42  
43  
44  
45  
46  
47  
48  
49  
50  
51  
52  
53  
54  
55  
56  
57  
58  
59  
60



**Table 1.** Spectral data in support of tautomeric equilibrium and open RAHB.

Row	1 OH/NH-O ensemble			2 OH/NH-O ensemble		
1.	<sup>1</sup> H7 ppm	9.64	8.97	9.05	8.74	
2.	<sup>1</sup> H8 ppm	15.24	13.20	14.19	11.32	
22.	<sup>1</sup> H7- <sup>1</sup> H8 coupling (Hz)	9.0	13.7	10.7	14.4	
3.	<sup>13</sup> C1 ppm	179.3	183.3	184.0	184.1	
4.	<sup>15</sup> N8 ppm	-197.9	-233.8	-229.4	-243.3	
24.	<sup>1</sup> H8- <sup>15</sup> N8 coupling (Hz)	67.2	89.5	84.2	91.2	
5.	<sup>1</sup> H7 Integr. Ratio (%)	94	6	85	15	
6.	Tautomeric NH-O% <sup>a</sup>	65		96		
7.	Overall population (%)	33	61	4	81	15
8.	NICS(1) <b>a</b>	-9.74	-4.27	-6.66	-2.66	-1.26
9.	HOMED <b>a</b>	0.924	0.762	0.876	0.714	0.646
10.	HOMED <b>q</b>	0.849	0.892	0.860	0.884	
11.	HOMED <b>a</b> (from xray)		0.873		0.795	
12.	HOMED <b>q</b> (from xray)		0.953		0.926	
13.	HOMED <b>q'</b>		0.937			0.906
14.	HOMED <b>c</b>	0.977	0.983	0.977	0.983	0.983
15.	NICS(1) <b>c</b>	-13.24	-9.35	-13.42	-9.37	-9.54
16.	NICS(1) <b>b</b>	-10.02	-9.04	-12.91	-11.20	-10.50

All energetic (kcal/mol, 298 K), geometric and NMR shielding calculations performed at B3LYP/6-311+g(d,p). NICS(1), HOMED values calculated for the 6-membered ring indicated by (**a**). NICS(1) values are reported as the negative isotropic shielding of a ghost atom 1.0 Å above the plane of the ring. HOMED: 0.0–0.4, 0.4–0.8, and 0.8–1.0 signify weak, moderate, and strong delocalization respectively. See SI for methods to calculate HOMED. All <sup>15</sup>N chemical shifts are referenced to CH<sub>3</sub>NO<sub>2</sub>. Experimental energy values measured by variable temperature NMR (see SI for details). <sup>a</sup>NH-O% = [<sup>1</sup>J<sub>NH</sub>/(96 Hz) × 100%].

#### D. Quantification of tautomeric population

The  $^1\text{H}$  NMR spectra were integrated to quantify the relative amounts of **OH/NH-O** and **NH-N** and showed that the **NH-N** form represents 6% and 15% of the total molecules in solution for **1** and **2**, respectively (row 5). Based on these populations, we determined the  $\Delta G^0$  difference between the **OH/NH-O** ensemble and the **NH-N** form at 298K to be 1.62 and 1.01 kcal/mol for **1** and **2**, respectively.

The relative amount of **OH** versus **NH-O** form within the **OH/NH-O** ensemble (the NH-O%, Table 1, row 6), can be estimated by measuring how closely the  $^1J_{\text{NH}}$  value of NH8 corresponds to an idealized  $^1J_{\text{NH}}$  value of 96Hz.<sup>44,51,52</sup> Numerous studies make use of  $^{13}\text{C}$  and  $^{17}\text{O}$  chemical shifts to estimate the %NH-O form, but there is often disagreement between the methods used to calculate the final NH-O%.<sup>16,53-55</sup> Indeed, recent theoretical studies suggest the NMR chemical shift of atoms within the RAHB is not a reliable proxy for determining the equilibrium.<sup>56,57</sup> Furthermore, the electron withdrawing nature of the heterocycles in **1** and **2** will also perturb the chemical shifts. Therefore, chemical shift is likely an inappropriate metric in our system. Thus, the %NH-O form within the **OH/NH-O** ensemble is most accurately determined from the  $^1J_{\text{NH}}$  coupling values that have historically been a more reliable indicator than  $^3J_{\text{H7-H8}}$  coupling values.<sup>58</sup>

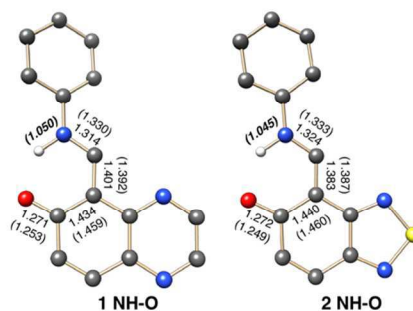


**Figure 4.** Single crystal X-ray diffraction structures of **1 NH-O** and **2 NH-O** comparing experimental and calculated (in brackets) bond lengths. Heavy-atom bond lengths were calculated using molecular DFT B3LYP/6-311+g(d,p). The H8 position and N8-H8 bond lengths were predicted with dispersion-corrected plane-wave DFT calculations with heavy atom positions fixed from single X-ray diffraction. Bond lengths for **2 NH-O** are an average of two structurally independent molecules in the asymmetric unit (s.u. are 0.004 for **1 NH-O** and 0.003 Å for **2 NH-O**). Anisotropic thermal ellipsoids depicted in (Figure S17).

The  $^1J_{\text{NH}}$  coupling values were measured for **1** and **2** using  $^1\text{H}\{^{15}\text{N}\}$  HMBC NMR on a cryoprobe 800 MHz spectrometer and  $^1J_{\text{NH}}$  was found to be 67.2 Hz and 84.2 Hz for **1** and **2** respectively (Figure 3, Table 1 row 4). The measured  $^1J_{\text{NH}}$  were converted to %NH-O via the equation %NH-O = [ $^1J_{\text{NH}}/(96 \text{ Hz}) \times 100\%$ ] (row 6). The  $^1J_{\text{NH}}$  coupling values were also measured for the **NH-N** form in each case. Both **1 NH-N** and **2 NH-N** show nearly identical  $^1J_{\text{NH}}$  ( $^{15}\text{N8}-^1\text{H8}$ ) coupling values of 89.5 and 91.2 Hz, respectively (row 4), which suggests that both **NH-N** forms exist, to the same extent, with the proton predominantly on N8. These measured  $^1J_{\text{NH}}$  are consistent with computational results that show proton transfer to the nitrogen atom in the heterocycle is energetically unfavorable (Figure S20). These results indicate that the geometry of the hydrogen bond and the basicity of the heterocyclic nitrogen (see  $pK_{\text{aH}}$  values of the parent heterocycles, Scheme 1) are unlikely to play a large role in the stability of the RAHB within **NH-N** because the heterocyclic nitrogen atoms do not appear to interact very strongly with H8.

#### E. Energetic balance of tautomers

The data from row 5 and 6 in Table 1 can be used to estimate the overall population of tautomers in solution (row 7) by multiplying the %NH-O for each **OH/NH-O** ensemble (row 6) by the integration value for  $^1\text{H7}$  (row 5). The values of NH-O% (Table 1, row 6) further confirm that the **NH-O** form is the majority form within the **OH/NH-O** ensemble for both **1** and **2**. Interestingly, however, the **1 OH/NH-O** ensemble is closer to parity, with the **1 NH-O** form slightly dominant, while the **2 OH/NH-O** ensemble is almost completely dominated by the **2 NH-O** form. These results align with the smaller calculated energy difference between **1 OH** and **1 NH-O** (1.28 kcal/mol) versus **2 OH** and **2 NH-O** (2.96 kcal/mol) at 298 K. Similarly, using variable temperature NMR, we determined the  $\Delta G^0$  at 298K to be  $-1.62$  and  $-1.01$  kcal/mol for **1** and **2** respectively to confirm

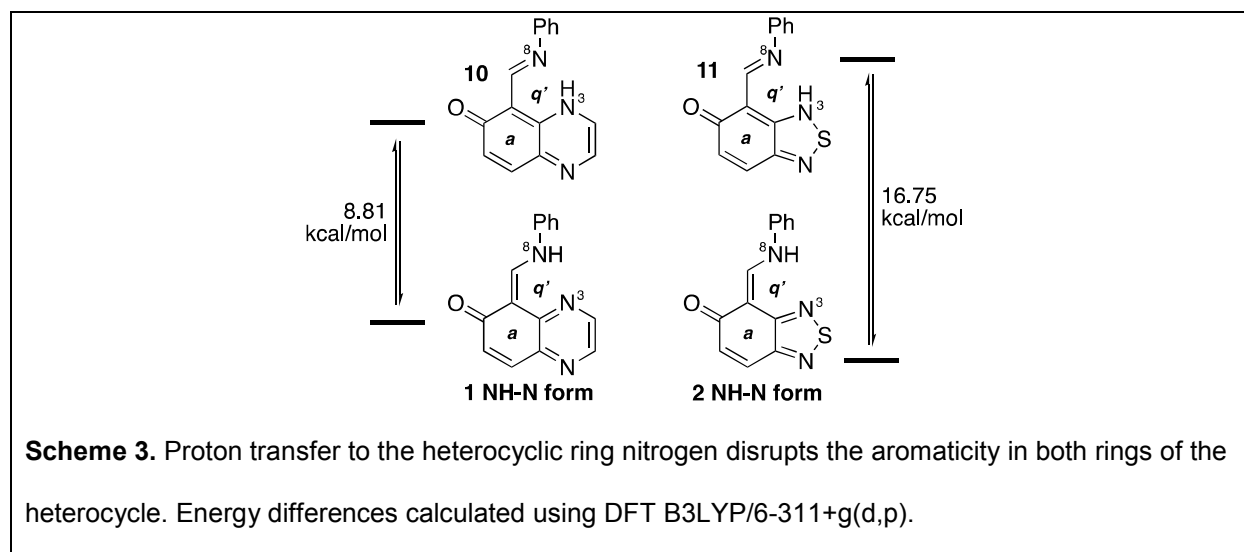
#### F. $\pi$ -Delocalization and competing aromaticity

We sought to investigate the reason behind the difference in the tautomeric equilibria of **OH**, **NH-O** and **NH-N** between **1** and **2**. As mentioned previously, the basicity of the heterocyclic nitrogen atoms (Scheme 1) does not appear to play a major role. Likewise, the inherent  $pK_{\text{a}}$  of the OH groups in each heterocycle (**3** and **4**, Figure 2) are so similar, we propose that the acidity—and the electron-withdrawing capacity of the heterocycles—plays very little role in the balance of tautomers. We therefore turned to investigate the role that aromaticity in rings **a**, **q** and **q'** might play in **1** and **2** (Table 1, rows 8–13).

1  
2  
3 Briefly, the aromaticity of a molecule can be estimated using computational chemistry to calculate  
4 the Nucleus Independent Chemical Shift (NICS) of a dummy atom placed 1 Å above the plane aromatic  
5 ring.<sup>59</sup> The more negative the NICS value, the more aromatic the ring (full NICS plots from 0–4 Å can be  
6 found in the SI, Figure S21). Alternatively, the Harmonic Oscillator Model of Electron Delocalization  
7 (HOMED)<sup>60</sup> is a geometry-based measure of aromaticity in which the closer the HOMED value is to 1, the  
8 more aromatic the molecule. An older index, HOMA<sup>61</sup> is prevalent in the literature of RAHB, and HOMA  
9 values have also been calculated and can be found in the SI (Table S3). We elected to go with HOMED  
10 in place of HOMA because HOMED is derived from computationally determine structural parameter, and  
11 we sought to cancel out any potential computational errors with the computed structures for **1** and **2**.

12  
13 In general, for compounds **1** and **2**, ring **a** loses aromaticity upon tautomerizing from the **OH** form  
14 to the **NH-O** form as indicated by both NICS(1) and HOMED methods (Table 1, rows 8 and 9). The  
15 aromaticity in ring **a** for the **OH** forms, however, is greater for **1** than for **2**. Thus, there is a smaller  
16 sacrifice of aromaticity in ring **a** for **2** upon tautomerization to the **NH-O** form, which explains why **2** exists  
17 in the **NH-O** form to a greater extent than **1**. Likewise, a small increase in the aromaticity of quasi-  
18 aromatic ring **q** is observed for both compounds upon tautomerization to **NH-O** (row 10). This observation  
19 aligns with previous reports that show ring **q** always displays significantly less change in its index of  
20 aromaticity relative to the sacrifice of aromaticity in ring **a** to form the RAHB.<sup>16</sup> The overall trend of this  
21 data is mirrored in the HOMED indices calculated from the X-ray crystal structures of **1** and **2** (rows 11  
22 and 12).

23  
24 For the **NH-N** forms, the quasiaromatic ring **q'** display high aromatic character according to  
25 HOMED indices (row 13), while ring **a** in each case loses still more aromatic character (row 9) relative to  
26 the **NH-O** forms. Again, we attribute the lower aromaticity in ring **a** of **2** as the reason that **2** displays more  
27 of the **NH-N** form in solution compared to **1**.



These results suggest that acid-base effects play very little role in determining the equilibrium of **1** and **2**, and the equilibrium is chiefly governed by aromaticity. We further propose that aromaticity considerations account for why proton transfer from N8 to N3 does not occur (described in section C above) (Scheme 3). The energy difference between **1 NH-N** to **10** and **2 NH-N** to **11** is too large to have an appreciable concentration at equilibrium. Tautomerization to form either **10** or **11** disrupts the aromaticity of both rings in the heterocycle because of  $\pi$ -delocalization to form the new  $q'$  N8-HN3 quasiaromatic ring. We propose that this aromatic disruption is the main factor responsible for the large energy difference.

Finally, rings **b** and **c** appear to be largely spectators in this isomerization process (Table 1, rows 14-16). HOMED values for ring **c** (row 14) indicate no change in aromaticity during tautomerization. The NICS(1) values (row 15), however, show a slight decrease in aromaticity of ring **c** upon tautomerization to the **NH-O** and **NH-N** forms which is likely due to changes in conjugation along the RAHB which alters conjugation effects and electron density within ring **c**. HOMED values were not calculated for ring **b** because N-S bonds have not been parameterized for analysis.<sup>60</sup> Alternatively, NICS(1) values were calculated for compounds **1** and **2** (row 16). In general, ring **b** in both **1** and **2** experiences very little change in aromaticity across the different tautomers. Comparison between ring **b** of **1** and **2** is not appropriate because of the different ring sizes (6-membered vs 5-membered) in **1** and **2**. 5-Membered rings typically appear 'more aromatic' than 6-member rings because the NICS measurement quantifies

1  
2  
3 the magnetic field at the center of the ring. Thus, the field is enhanced as the  $\pi$ -bonds move closer to the  
4 point where NICS is being measured.  
5  
6  
7

## 8 9 **CONCLUSION**

10 Collectively, these results indicate that resonance-assisted hydrogen bonds (RAHB) can be  
11 opened up provided there is a suitable Lewis base to stabilize the proton. This effect has not been  
12 observed before in the literature of RAHB, and we provide the first characterization of such an effect to  
13 open a RAHB to form quasi-aromatic ring **q'**. We also sought to investigate the effect that acid-base  
14 interactions might have on the RAHB and the equilibrium in Figure 1. We selected quinoxaline (**3**) and  
15 benzothiadiazole (**4**) as the base heterocycles for this analysis because our measurements revealed  
16 them to have very similar  $pK_a$  values for their hydroxyl groups. These similar acidities, allowed us to  
17 isolate the aromaticity in ring **a** as the chief factor in determining the balance of tautomers in the **OH/NH-**  
18 **O** equilibrium ensemble. Similarly, the difference in basicity of the heterocyclic nitrogen atoms in the **NH-**  
19 **N** tautomer did not appear to influence the position of the proton in the RAHB (based on  $^1J_{N8-H8}$  coupling  
20 values in **NH-N**. These findings supports the primacy of aromaticity and  $\pi$ -delocalization in determining  
21 the tautomeric position in RAHB.  
22  
23  
24  
25  
26  
27  
28  
29  
30  
31  
32

## 33 **EXPERIMENTAL SECTION**

34 **Materials.** Silica gel (40  $\mu$ m) was purchased from Grace Davison. All solvents used for photophysical  
35 experiments were reagent grade. 4-chlorobenzene-1, 2-diamine (**1**) was purchased from Oakwood  
36 Chemicals, Palladium catalyst from Strem Chemicals, Hexamethylenetetramine from Alfa Aesar. All other  
37 reagents were purchased from Sigma Aldrich and used without further purification.  
38  
39  
40  
41  
42

43 **General Method. NMR Spectroscopy:**  $^1\text{H}$  and  $^{13}\text{C}$  NMR spectra for all compounds were acquired in  
44 deuterated solvents (as indicated) on a Bruker Spectrometer at the field strengths reported in the text.  
45 The chemical shift data are reported in units of  $\delta$  (ppm) relative to residual solvent. 1D  $^1\text{H}$  NMR and  $^1\text{H}-$   
46  $^{13}\text{C}$  HMBC NMR spectra were obtained using a 600 MHz Bruker Avance III spectrometer. Quantitative 1D  
47  $^1\text{H}$  NMR spectra were obtained at different temperatures for the thermodynamic analysis using long  
48 recycle delays of 100 s ( $> 5 \times T_1$ ) between subsequent scans.  $^1\text{H}-^{15}\text{N}$  HMBC NMR spectra were recorded  
49 using a 700 MHz Bruker Avance II NMR spectrometer. **IR Spectroscopy:** Solutions of **1** and **2** in  $\text{CCl}_4$   
50  
51  
52  
53  
54  
55  
56  
57  
58  
59  
60

1  
2  
3 were dropped onto KBr plates before collection of the spectrum on a Bruker Vertex 80 FTIR  
4 spectrometer.  
5

6  
7 **General Computational.** All molecules considered were optimized at the nonlocal three-parameter  
8 hybrid B3LYP level of theory<sup>62,63</sup> under the 6-311+g(d,p) basis set. Vibrational analysis of each structure  
9 verified the existence of a minima due to the absence of imaginary frequencies. All calculations were  
10 carried out with the Gaussian 09 package.<sup>64</sup> Additionally, the hybrid CAM-B3LYP<sup>65</sup> and M06-2X<sup>66</sup>  
11 functionals were also for their ability to model charge transfer reactions and weak non-covalent  
12 interactions, respectively (Table S4). However, recent literature precedent has utilized the B3LYP  
13 functional to model proton transfer reactions and isomerizations.<sup>67-69</sup>

14  
15  
16  
17  
18  
19  
20 HOMED values were obtained by using equation 1 where j indicates the bond type.

$$21 \quad \text{HOMED} = 1 - \frac{\alpha \sum (R_{opt,j} - R_{i,j})^2}{n}$$

22  
23  
24  
25  $R_{opt}$  and  $\alpha$  values used were from Raczyńska et. al. initial report of HOMED:<sup>60</sup> CC( $R_{opt} = 1.394$ ,  $\alpha_{2i} =$   
26 88.09), CN(1.334, 91.60), CO(1.281, 75.00).  
27

28  
29 Plane-wave DFT calculations were performed on compounds 1 and 2 using CASTEP.<sup>70</sup> The X-ray crystal  
30 structures were used to fix the heavy atom positions and the hydrogen atom positions were optimized. All  
31 calculations used the Perdew-Burke-Ernzerhof (PBE) functional<sup>71</sup> with the Tkatchenko-Scheffler (TS)  
32 dispersion correction scheme<sup>72</sup> and ultra-soft pseudopotentials generated *on-the-fly*. The wavefunctions  
33 were expanded using a plane-wave basis set with a kinetic energy cut-off of 630 eV. A Monkhorst-Pack  
34 grid with a  $k$ -point spacing of 0.07 Å<sup>-1</sup> was used to calculate the integrals over the Brillouin zone.  
35  
36  
37  
38

39  
40 **Synthesis of 6-chloroquinoxaline (6).** The diamine **5** (428 mg, 3.00 mmol) was added to a solution of  
41 glyoxal in water and stirred at RT for 1h. Upon completion (determined by TLC), the reaction was  
42 extracted with DCM, dried over MgSO<sub>4</sub> and concentrated *in vacuo*. <sup>1</sup>H NMR of the crude product matched  
43 previously reported literature.<sup>37</sup> <sup>1</sup>H NMR (CDCl<sub>3</sub>, 600Hz):  $\delta$  8.83 (d,  $J = 6$  Hz, 2H),  $\delta$  8.09 (s, 1H),  $\delta$  8.03  
44 (d,  $J = 9$  Hz, 1H),  $\delta$  7.70 (d,  $J = 8.4$  Hz, 1H).  
45  
46  
47  
48  
49

50  
51 **Synthesis of quinoxalin-6-ol (3).** Compound **6** (164 mg, 1.0 mmol), K<sub>2</sub>CO<sub>3</sub> (414 mg, 3.0 mmol) and  
52 precatalyst Pd-*t*-BuXphos (40 mg, 5.0 mol %) (see SI for structure) were added together in a vial, then  
53 vacuumed and back-filled with nitrogen three times. Next, 5 mL of degassed DMF/water (5:1 v/v) was  
54 added. The reaction mixture was stirred at 115 °C for 4 h. Upon completion, the reaction was poured into  
55  
56  
57  
58  
59  
60

1  
2  
3 1M HCl and extracted with diethyl ether three times. The combined organic fractions were dried over  
4 MgSO<sub>4</sub> and concentrated *in vacuo*. The crude residue was triturated with hexane and DCM to give **3**  
5 (87.6 mg, 60% yield). <sup>1</sup>H NMR of the product matched previously reported literature.<sup>73</sup> <sup>1</sup>H NMR (DMSO,  
6 600Hz): δ 10.56 (s, OH, 1H), δ 8.77 (d, *J* = 2.4Hz, 1H), δ 8.67 (d, *J* = 2.4 Hz, 1H), δ 7.90 (d, *J* = 9 Hz,  
7 1H), δ 7.42 (dd, *J* = 9 Hz, 2.7 Hz, 1H), δ 7.24 (d, *J* = 2.7 Hz, 1H).  
8  
9  
10  
11

12 **Synthesis of (Z)-5-((phenylamino)methylene)quinoxalin-6(5H)-one (1).** Compound **3** (1.0 mmol, 146  
13 mg) and NaOH (4.0 mmol, 160 mg) were dissolved in 2.0 mL of water by heating to 100 °C for 30 min.  
14 Then 1.5 mL chloroform was added with vigorous stirring. More NaOH was added to keep the pH of the  
15 reaction at 10 (determined with pH paper). Upon completion, the reaction was acidified to pH 6, and the  
16 solid was collected by filtration. The crude product was condensed with excess aniline (1.0 mL) in 5.0 mL  
17 DCM at 45 °C, in a seal tube for 1h and monitored by TLC. The reaction was quenched with 1M HCl. The  
18 organic layer was separated, concentrated under vacuum and purified by silica gel column  
19 chromatography (1:5 EtOAc:Hex) to obtain the final product **1** (99 mg, 40%). <sup>1</sup>H NMR (DMSO, 600 Hz):  
20 δ 9.67 (s, 1H), δ 8.73 (s, 1H), δ 8.63 (s, 1H), δ 7.92 (d, *J* = 9.68 Hz, 1H), δ 7.58 (d, *J* = 7.4 Hz, 2H), δ 7.50  
21 (t, *J* = 7.4 Hz, 2H), δ 7.34 (t, *J* = 7.4 Hz, 1H), δ 7.15 (d, *J* = 9.68 Hz, 1H). <sup>13</sup>C NMR (DMSO, 150 Hz): δ  
22 176.3, 153.5, 144.5, 141.6, 140.9, 137.1, 136.9, 129.9, 129.3, 127.0, 119.7, 108.0. HRMS (ESI, TOF)  
23 *m/z*: [M +H]<sup>+</sup> Calcd for C<sub>15</sub>H<sub>11</sub>N<sub>3</sub>O 250.0975, found 250.0975.  
24  
25  
26  
27  
28  
29  
30  
31  
32  
33  
34

35 **Synthesis of 5-chlorobenzo[c][1,2,5]thiadiazole (7).** Based on a previously reported procedure,<sup>38</sup> 4-  
36 chlorobenzene-1,2-diamine (1.43 g, 10 mmol) was added to a flame dried round bottom flask and placed  
37 under nitrogen. SOCl<sub>2</sub> (8.2 g, 5.0 mL, 68 mmol) and 0.220 mL of concentrated H<sub>2</sub>SO<sub>4</sub> (405 mg, 4.1 mmol)  
38 were subsequently added. The reaction mixture was refluxed for 6 h and cooled to RT. The solution was  
39 diluted with water and extracted with EtOAc. The EtOAc phase was repeatedly washed with water until  
40 the aqueous phase was no longer acidic by pH paper. The organic phase was dried over MgSO<sub>4</sub> and  
41 concentrated under vacuum. The crude mixture was purified by silica gel flash column chromatography  
42 (5:1, Hexanes: EtOAc, R<sub>f</sub> = 0.7) to afford the product **7** as a reddish brown solid (1.2 g, 70%). <sup>1</sup>H NMR  
43 (CDCl<sub>3</sub>, 400 MHz) δ 7.85 (d, *J* = 4 Hz, 1H), δ 7.77 (d, *J* = 12 Hz, 1H), δ 7.38 (dd, *J* = 4 Hz, 6 Hz, 1H).  
44  
45  
46  
47  
48  
49  
50  
51  
52  
53 Spectra of product match those previously reported.<sup>38</sup>  
54  
55  
56  
57  
58  
59  
60



1  
2  
3 **Synthesis of benzo[c][1,2,5]thiadiazol-5-ol (4).** Compound **7** (17.0 mg, 0.10 mmol), KOH (17.0 mg,  
4 0.30 mmol) and 3.96 mg (5% mmol) of Pd-*t*-BuXPhos precatalyst (see SI for structure) were added to a  
5 flame dried round bottom flask. The reaction flask was evacuated and back filled with nitrogen three times  
6 before 36  $\mu$ L of degassed water:DMF (1:9 v:v) was added. The reaction was stirred for 18h at 80 °C.  
7  
8 Upon cooling to RT, the reaction was diluted with water, acidified with 1M HCl and extracted with EtOAc  
9 three times. The combined organic fractions were dried over MgSO<sub>4</sub> and concentrated under vacuum.  
10  
11 The residue was purified by silica gel flash column chromatography (start with 5:1 and gradient to 1:1,  
12 Hexanes:EtOAc, R<sub>f</sub> = 0.2) to afford a light yellow solid (10.6 mg, 70%). <sup>1</sup>H NMR ((CD<sub>3</sub>)<sub>2</sub>CO, 600 Hz),  $\delta$   
13 7.88 (d, *J* = 9.6 Hz, 1H),  $\delta$  7.37 (dd, *J* = 2.40 Hz, 9.6 Hz, 1H),  $\delta$  7.22 (d, *J* = 2.4 Hz, 1H). Spectra of  
14 product match those previously reported.<sup>39</sup>

15  
16 **Synthesis of 5-hydroxybenzo[c][1,2,5]thiadiazole-4-carbaldehyde (9).** Based on a previously reported  
17 procedure,<sup>42</sup> **4** (76 mg, 0.50 mmol) and hexamethylenetetramine (HMTA) (70 mg, 0.50 mmol) were  
18 dissolved in 1.0 mL of TFA in a round bottom flask at RT. After the consumption of starting material  
19 (tracked by TLC), the reaction was heated to 70 °C for 48 h. Upon cooling to RT, the reaction was  
20 quenched with water and the mixture was extracted with ethyl acetate. The EtOAc portion was dried over  
21 MgSO<sub>4</sub> and concentrated *in vacuo*. The residue was purified by silica gel column chromatography (1:1,  
22 Hexanes:EtOAc, R<sub>f</sub> = 0.35) to afford a crude orange yellow product that was used without further  
23 purification (44 mg, 49.0 %). <sup>1</sup>H NMR (CDCl<sub>3</sub>, 600 MHz)  $\delta$  13.0 (br s, OH, 1H),  $\delta$  10.7 (s, CHO, 1H),  $\delta$   
24 8.11 (d, *J* = 9.6 Hz, 1H),  $\delta$  7.33 (d, *J* = 9.6 Hz, 1H). <sup>13</sup>C NMR (CDCl<sub>3</sub>, 150 MHz)  $\delta$  193.7, 167.4, 154.2,  
25 150.3, 130.0, 124.8, 108.82. HRMS (ESI, TOF) *m/z*: [M - H]<sup>-</sup> Calcd for C<sub>7</sub>H<sub>4</sub>N<sub>2</sub>O<sub>2</sub>S 178.9921, found [M-H]  
26 178.9897.

27  
28 **Synthesis of (Z)-4-((phenylamino) methylene)benzo[c][1,2,5]thiadiazol-5(4H)-one (2).** Compound **9**  
29 (108 mg, 0.60 mmol) was dissolve in EtOH (3.0 mL, 0.50 M in 9). Aniline (54 mg, 0.60 mmol) was added,  
30 and the reaction was warmed to 40 °C and tracked by TLC until completion. The reaction was poured into  
31 water and extracted with ethyl acetate. The EtOAc portion was dried over MgSO<sub>4</sub> and purified by silica gel  
32 flash chromatography (5:1, Hexanes:EtOAc, R<sub>f</sub> = 0.45) to give a quantitative yield of **2** (153 mg, 99%). <sup>1</sup>H  
33 NMR (CDCl<sub>3</sub>, 400 Hz):  $\delta$  14.2 (d, *J* = 10.4 Hz, 1H, H8),  $\delta$  8.90 (d, *J* = 11.2 Hz, 1H, H7),  $\delta$  7.63 (d, *J* = 9  
34 Hz, 1H),  $\delta$  7.36 (m, 2H),  $\delta$  7.33 (m, 2H),  $\delta$  7.2 (t, *J* = 7.4 Hz, 1H). <sup>13</sup>C NMR (CDCl<sub>3</sub>, 100 Hz):  $\delta$  183.1,  
35  
36  
37  
38  
39  
40  
41  
42

156.4, 149.4, 149.0, 138.5, 131.9, 129.9, 129.3, 126.6, 118.3, 104.7. HRMS (ESI, TOF)  $m/z$ :  $[M + H]^+$   
Calcd for  $C_{13}H_9N_3OS$  256.0539, found (M+H) 256.0568.

## ASSOCIATED CONTENT

The Supporting Information is available free of charge on the ACS Publications website at DOI:  
Structures of catalysts discussed in the main text, DFT calculations, computational analyses, pKa studies  
and NMR spectra. X-ray crystal structures have been deposited in the Cambridge Crystallographic Data  
Centre (1844550 and 1844551).

## AUTHOR INFORMATION

### Corresponding Author

\*Email: [bvv@iastate.edu](mailto:bvv@iastate.edu)

### ORCID

Brett VanVeller: [0000-0002-3792-0308](https://orcid.org/0000-0002-3792-0308)

### Notes

The authors declare no competing financial interest.

## ACKNOWLEDGMENTS

We are grateful for support of this work by Iowa State University of Science and Technology and a Pfizer  
Global ASPIRE Award (WI216840).

## REFERENCES

- (1) Raczyńska, E. D.; Kosińska, W.; Ośmiałowski, B.; Gawinecki, R. Tautomeric Equilibria in Relation to Pi-Electron Delocalization. *Chem. Rev.* **2005**, *105*, 3561.
- (2) Phillips, R. Chemistry and Diversity of Pyridoxal-5'-Phosphate Dependent Enzymes. *Biochim Biophys Acta.* **2015**, *1854*, 1167.
- (3) Sharif, S.; Denisov, G. S.; Toney, M. D.; Limbach, H. H. Nmr Studies of Solvent-Assisted Proton Transfer in a Biologically Relevant Schiff Base: Toward a Distinction of Geometric and Equilibrium H-Bond Isotope Effects. *J. Am. Chem. Soc.* **2006**, *128*, 3375.
- (4) Christen, P.; Metzler, P. E.; Eds *Transaminases*; Wiley: New York, 2005.
- (5) Kaplan, J. P.; Raizon, B. M.; Desarmenien, M.; Feltz, P.; Headley, P. M.; Worms, P.; Lloyd, K. G.; Bartholini, G. New Anticonvulsants: Schiff Bases Of .Gamma.-Aminobutyric Acid And .Gamma.-Aminobutyramide. *J. Med. Chem.* **1980**, *23*, 702.
- (6) Krause, M.; Rouleau, A.; Stark, H.; Luger, P.; Lipp, R.; Garbarg, M.; Schwart, J. C.; Schunack, W. Synthesis, X-Ray Crystallography, and Pharmacokinetics of Novel Azomethine Prodrugs of (R)-.Alpha.-Methylhistamine: Highly Potent and Selective Histamine H3 Receptor Agonists. *J. Med. Chem.* **1995**, *38*, 4070.

- (7) Maekawa, T.; Yamamoto, S.; Igata, Y.; Ikeda, S.; Watanabe, T.; Shiraishi, M. Synthesis and Biological Activity of Novel 2-(Alpha-Alkoxyimino) Benzylpyridine Derivatives as K<sup>+</sup> Channel Openers. *Chem. Pharm. Bull. (Tokyo)* **1994**, *45*, 1994.
- (8) Grozinger, C. M.; Chao, E. D.; Blackwell, H. E.; Moazed, D.; Schreiber, S. L. Identification of a Class of Small Molecule Inhibitors of the Sirtuin Family of Nad-Dependent Deacetylases by Phenotypic Screening. *J Biol Chem* **2001**, *276*, 38837.
- (9) Hu, J.; Jing, H.; Lin, H. Sirtuin Inhibitors as Anticancer Agents. *Future Med Chem* **2014**, *6*, 945.
- (10) Ota, H.; Tokunaga, E.; Chang, K.; Hikasa, M.; Iijima, K.; Eto, M.; Kozaki, K.; Akishita, M.; Ouchi, Y.; Kaneki, M. Sirt1 Inhibitor, Sirtinol, Induces Senescence-Like Growth Arrest with Attenuated Ras-Mapk Signaling in Human Cancer Cells. *Oncogene* **2006**, *25*, 176.
- (11) Peck, B.; Chen, C. Y.; Ho, K. K.; Di Fruscia, P.; Myatt, S. S.; Coombes, R. C.; Fuchter, M. J.; Hsiao, C. D.; Lam, E. W. Sirt Inhibitors Induce Cell Death and P53 Acetylation through Targeting Both Sirt1 and Sirt2. *Mol Cancer Ther.* **2010**, *9*, 844.
- (12) Kojima, K.; Ohhashi, R.; Fujita, Y.; Hamada, N.; Akao, Y.; Nozawa, Y.; Deguchi, T.; Ito, M. A Role for Sirt1 in Cell Growth and Chemoresistance in Prostate Cancer Pc3 and Du145 Cells. *Biochem Biophys Res Commun* **2008**, *373*, 423.
- (13) Jin, K. L.; Park, J. Y.; Noh, E. J.; Hoe, K. L.; Lee, J. H.; Kim, J. H.; Nam, J. H. The Effect of Combined Treatment with Cisplatin and Histone Deacetylase Inhibitors on Hela Cells. *J Gynecol Oncol.* **2010**, *21*, 262.
- (14) Kalle, A. M.; Mallika, A.; Badiger, J.; Alinakhi; Talukdar, P.; Sachchidanand Inhibition of Sirt1 by a Small Molecule Induces Apoptosis in Breast Cancer Cells. *Biochem Biophys Res Commun.* **2010**, *401*, 13.
- (15) Kanda, T.; Sasaki, R.; Nakamoto, S.; Haga, Y.; Nakamura, M.; Shirasawa, H.; Okamoto, H.; Yokosuka, O. The Sirtuin Inhibitor Sirtinol Inhibits Hepatitis a Virus (Hav) Replication by Inhibiting Hav Internal Ribosomal Entry Site Activity. *Biochem Biophys Res Commun.* **2015**, *466*, 567.
- (16) Gawinecki, R.; Kuczek, A.; Kolehmainen, E.; Ośmiałowski, B.; Krygowski, T. M.; Kauppinen, R. Influence of Bond Fixation in Benzo-Annulated N-Salicylideneanilines and Their Ortho-C(=O)X Derivatives (X = Ch<sub>3</sub>, Nh<sub>2</sub>, Och<sub>3</sub>) on Tautomeric Equilibria in Solution. *J Org Chem.* **2007**, *72*, 5598.
- (17) Filarowski, A.; Koll, A.; Glowiak, T. Low Barrier Hydrogen Bonds in Sterically Modified Schiff Bases. *J. Chem. Soc., Perkin Trans. 2* **2002**, 835.
- (18) Filarowski, A. Intramolecular Hydrogen Bonding in O-Hydroxyaryl Schiff Basest. *J. Phys. Org. Chem.* **2005**, *18*, 686.
- (19) Filarowski, A.; Kochel, A.; Cieslik, K.; Koll, A. Steric and Aromatic Impact on Intramolecular Hydrogen Bonds in O-Hydroxyaryl Ketones and Ketimines. *J. Phys. Org. Chem.* **2005**, *18*, 986.
- (20) Filarowski, A.; Kochel, A.; Kluba, M.; Kamounah, F. S. Structural and Aromatic Aspects of Tautomeric Equilibrium in Hydroxy Aryl Schiff Bases. *J. Phys.Org. Chem.* **2008**, *21*, 939.
- (21) Krygowski, T. M.; Szatyłowicz, H.; Stasyuk, O. A.; Dominikowska, J.; Palusiak, M. Aromaticity from the Viewpoint of Molecular Geometry: Application to Planar Systems. *Chem. Rev.* **2014**, *114*, 6383.

- 1  
2  
3 (22) Karabiyik, H.; Sevinçek, R.; Petek, H.; Aygün, M. Aromaticity Balance, Pi-Electron  
4 Cooperativity and H-Bonding Properties in Tautomerism of Salicylideneaniline: The Quantum  
5 Theory of Atoms in Molecules (Qtaim) Approach. *J. Mol. Model.*  
6 **2011**, *17*, 1295.
- 7  
8 (23) Gilli, G.; Bellucci, F.; Ferretti, V.; Bertolasi, V. Evidence for Resonance-Assisted  
9 Hydrogen-Bonding from Crystal-Structure Correlations on the Enol Form of The .Beta.-Diketone  
10 Fragment. *J. Am. Chem. Soc.* **1989**, *111*, 1023.
- 11  
12 (24) Bertolasi, V.; Gilli, P.; Ferretti, V.; Gilli, G. Evidence for Resonance-Assisted  
13 Hydrogen-Bonding .2. Intercorrelation between Crystal-Structure and Spectroscopic Parameters  
14 in 8 Intramolecularly Hydrogen-Bonded 1,3-Diaryl-1,3-Propanedione Enols. *J. Am. Chem. Soc.*  
15 **1991**, *113*, 4917.
- 16  
17 (25) Gilli, P.; Bertolasi, V.; Ferretti, V.; Gilli, G. Evidence for Intramolecular N–H···O  
18 Resonance-Assisted Hydrogen Bonding in B-Enaminones and Related Heterodienes. A  
19 Combined Crystal-Structural, Ir and Nmr Spectroscopic, and Quantum-Mechanical Investigation.  
20 *J. Am. Chem. Soc.* **2000**, *122*, 10405.
- 21  
22 (26) Mahmudov, K. T.; Pombeiro, A. J. L. Resonance-Assisted Hydrogen Bonding as a  
23 Driving Force in Synthesis and a Synthone in the Design of Materials. *Chem. Eur. J.* **2016**, *22*,  
24 16356.
- 25  
26 (27) Sanz, P.; Mó, O.; Yáñez, M.; Elguero, J. *J. Phys. Chem. A* **2007**, *111*, 3585.
- 27  
28 (28) Gilli, P.; Pretto, L.; Bertolasi, V.; Gilli, G. Predicting Hydrogen-Bond Strengths  
29 from Acid-Base Molecular Properties. The Pk(a) Slide Rule: Toward the Solution of a Long-  
30 Lasting Problem. *Acc Chem Res* **2009**, *42*, 33.
- 31  
32 (29) Zubatyuk, R. I.; Volovenko, Y. M.; Shishkin, O. V.; Gorb, L.; Leszczynski, J.  
33 Aromaticity-Controlled Tautomerism and Resonance-Assisted Hydrogen Bonding in Heterocyclic  
34 Enaminone-Iminoenol Systems. *J. Org. Chem.* **2007**, *72*, 725.
- 35  
36 (30) Krygowski, T. M.; Bankiewicz, B.; Czarnocki, Z.; Palusiak, M. Quasi-Aromaticity-  
37 What Does It Mean? *Tetrahedron* **2015**, *71*, 4895.
- 38  
39 (31) Gutierrez-Arzaluz, L.; Cortes-Guzman, F.; Rocha-Rinza, T.; Peon, J. Ultrafast  
40 Excited State Hydrogen Atom Transfer in Salicylideneaniline Driven by Changes in Aromaticity.  
41 *Phys. Chem. Chem. Phys.* **2015**, *17*, 31608.
- 42  
43 (32) Kolehmainen, E.; Osmialowski, B.; Krygowski, T. M.; Kauppinen, R.; Nissinen, M.;  
44 Gawinecki, R. Substituent and Temperature Controlled Tautomerism: Multinuclear Magnetic  
45 Resonance, X-Ray, and Theoretical Studies on 2-Phenacylquinolines. *Journal of the Chemical*  
46 *Society-Perkin Transactions 2* **2000**, *6*, 1259.
- 47  
48 (33) Kolehmainen, E.; Osmialowski, B.; Nissinen, M.; Kauppinen, R.; Gawinecki, R.  
49 Substituent and Temperature Controlled Tautomerism of 2-Phenacylpyridine: The Hydrogen  
50 Bond as a Configurational Lock of (Z)-2-(2-Hydroxy-2-Phenylvinyl)Pyridine. *J. Chem. Soc., Perkin*  
51 *Trans. 2* **2000**, 2185.
- 52  
53 (34) Gawinecki, R.; Kolehmainen, E.; Loghmani-Khouzani, H.; Osmialowski, B.; Lovasz,  
54 T.; Rosa, P. Effect of Pi-Electron Delocalization on Tautomeric Equilibria - Benzoannulated 2-  
55 Phenacylpyridines. *Eur. J. Org Chem.* **2006**, 2817.
- 56  
57 (35) Gilli, P.; Gilli, G. Hydrogen Bond Models and Theories: The Dual Hydrogen Bond  
58 Model and Its Consequences. *J Mol Struct* **2010**, *972*, 2.
- 59  
60

- 1  
2  
3 (36) Martinez, C. H.; Dardonville, C. Rapid Determination of Ionization Constants (Pka) by Uv Spectroscopy Using 96-Well Microtiter Plates. *ACS Med. Chem. Lett.* **2013**, *4*, 142.
- 4  
5 (37) Delpivo, C.; Micheletti, G.; Boga, C. A Green Synthesis of Quinoxalines and 2,3-Dihydropyrazines. *Synthesis* **2013**, *45*, 1546.
- 6  
7 (38) Yasuda, H.; Domitrovich, O. V. US. Pat. Appl. 20090149676 Publ, US12327506, June 11, 2009.
- 8  
9 (39) Cheung, C. W.; Buchwald, S. L. Palladium-Catalyzed Hydroxylation of Aryl and Heteroaryl Halides Enabled by the Use of a Palladacycle Precatalyst. *J. Org. Chem.* **2014**, *79*, 5351.
- 10  
11 (40) Wynberg, H. The Reimer-Tiemann Reaction. *Chem. Rev.* **1960**, *60*, 169.
- 12  
13 (41) Ferguson, L. N. The Synthesis of Aromatic Aldehydes. *Chem. Rev.* **1946**, *38*, 227.
- 14  
15 (42) Skonieczny, K.; Charalambidis, G.; Tasior, M.; Krzeszewski, M.; Kalkan-Burat, A.; Coutsolelos, A. G.; Gryko, D. T. General and Efficient Protocol for Formylation of Aromatic and Heterocyclic Phenols. *Synthesis* **2012**, *44*, 3683.
- 16  
17 (43) Witanowski, M.; Stefaniak, L.; Webb, G. A. Nitrogen Nmr Spectroscopy. *Annu. Rep. NMR Spectrosc.* **1993**, *25*, 1.
- 18  
19 (44) Salman, S. R.; Lindon, J. C.; Farrant, R. D.; Carpenter, T. A. Tautomerism in 2-Hydroxy-L-Naphthaldehyde Schiff-Bases in Solution and the Solid-State Investigated Using C-13 Nmr-Spectroscopy. *Magnetic Resonance in Chemistry* **1993**, *31*, 991.
- 20  
21 (45) Kascheres, C. M. The Chemistry of Enaminones, Diazocarbonyls and Small Rings: Our Contribution. *J. Braz. Chem. Soc.* **2003**, *14*, 945.
- 22  
23 (46) Ogawa, K.; Harada, J. Aggregation Controlled Proton Tautomerization in Salicylideneanilines. *J Mol Struct* **2003**, *647*, 211.
- 24  
25 (47) Buemi, G.; Zuccarello, F.; Venuvanalingam, P.; Ramalingam, M. Ab Initio Study of Tautomerism and Hydrogen Bonding of Beta-Carbonylamine in the Gas Phase and in Water Solution. *Theor Chem Acc* **2000**, *104*, 226.
- 26  
27 (48) Rybarczyk-Pirek, A. J.; Grabowski, S. J.; Malecka, M.; Nawrot-Modranka, J. Crystal and Molecular Structures of New Chromone Derivatives as Empirical Evidence of Intramolecular Proton Transfer Reaction; Ab Initio Studies on Intramolecular H-Bonds in Enaminones. *J. Phys. Chem. A* **2002**, *106*, 11956.
- 28  
29 (49) Ogawa, K.; Kasahara, Y.; Ohtani, Y.; Harada, J. Crystal Structure Change for the Thermochromy of N-Salicylideneanilines. The First Observation by X-Ray Diffraction. *J. Am. Chem. Soc.* **1998**, *120*, 7107.
- 30  
31 (50) Dziembowska, T.; Szafran, M.; Katrusiak, A.; Rozwadowski, Z. Crystal Structure of and Solvent Effect on Tautomeric Equilibrium in Schiff Base Derived from 2-Hydroxy-1-Naphthaldehyde and Methylamine Studied by X-Ray Diffraction, Dft, Nmr and Ir Methods. *J Mol Struct* **2009**, *929*, 32.
- 32  
33 (51) Sitkowski, J.; Stefaniak, L.; Dziembowska, T.; Grech, E.; Jagodzinska, E.; Webb, G. A. A Multinuclear Nmr Study of Proton Transfer Processes in Schiff Bases. *J. Mol. Struct* **1996**, *381*, 177.
- 34  
35 (52) Dudek, G. O. Nuclear Magnetic Resonance Studies of Keto-Enol Equilibria .4. Naphthalene Derivatives. *J. Am. Chem. Soc.* **1963**, *85*, 694.
- 36  
37  
38  
39  
40  
41  
42  
43  
44  
45  
46  
47  
48  
49  
50  
51  
52  
53  
54  
55  
56  
57  
58  
59  
60

(53) Alarcon, S. H.; Olivieri, A. C.; Sanz, D.; Claramunt, R. M.; Elguero, J. Substituent and Solvent Effects on the Proton Transfer Equilibrium in Anils and Azo Derivatives of Naphthol. Multinuclear Nmr Study and Theoretical Calculations. *J Mol Struct* **2004**, *705*, 1.

(54) Alarcon, S. H.; Olivieri, A. C.; Gonzalezzierra, M. C-13 Nmr Spectroscopic and Am1 Study of the Intramolecular Proton-Transfer in Anils of Salicylaldehyde and 2-Hydroxynaphthalene-1-Carbaldehyde. *J Chem Soc Perk T 2* **1994**, 1067.

(55) Zhuo, J. C. Nmr of Enaminones. Part 6 - O-17 and C-13 Nmr Study of Tautomerization in Schiff Bases. *Magn Reson Chem* **1999**, *37*, 259.

(56) Alkorta, I.; Elguero, J.; Mo, O.; Yanez, M.; Del Bene, J. E. Are Resonance-Assisted Hydrogen Bonds 'Resonance Assisted'? A Theoretical Nmr Study. *Chem Phys Lett* **2005**, *411*, 411.

(57) Alkorta, I.; Elguero, J.; Mo, O.; Yanez, M.; Del Bene, J. E. Do Coupling Constants and Chemical Shifts Provide Evidence for the Existence of Resonance-Assisted Hydrogen Bonds? *Mol Phys* **2004**, *102*, 2563.

(58) Dobosz, R.; Skotnicka, A.; Rozwadowski, Z.; Dziembowska, T.; Gawinecki, R. Stability of N-(Ortho-Hydroxynaphthylmethylene)Methylamines and Their Tautomers. *J Mol Struct* **2010**, *979*, 194.

(59) Chen, Z.; Wannere, C. S.; Corminboeuf, C.; Puchta, R.; Schleyer, P. Nucleus-Independent Chemical Shifts (Nics) as an Aromaticity Criterion. *Chem. Rev.* **2005**, *105*, 3842.

(60) Raczyńska, E. D.; Hallman, M.; Kolczyńska, K.; Stępniewski, T. M. On the Harmonic Oscillator Model of Electron Delocalization (Homed) Index and Its Application to Heteroatomic Pi-Electron Systems. *Symmetry* **2010**, *2*, 1485.

(61) Krygowski, T. M. Crystallographic Studies of Inter- and Intramolecular Interactions Reflected in Aromatic Character of Pi-Electron System. *J. Chem. Inf. Comput. Sci.* **1993**, *33*, 70.

(62) Becke, A. D. Density-Functional Thermochemistry .3. The Role of Exact Exchange. *J. Chem. Phys.* **1993**, *98*, 5648.

(63) Lee, C. T.; Yang, W. T.; Parr, R. G. Development of the Colle-Salvetti Correlation-Energy Formula into a Functional of the Electron-Density. *Phys. Rev. B* **1988**, *37*, 785.

(64) Gaussian 09, Revision A.02, M. J. Frisch, G. W. Trucks, H. B. Schlegel, G. E. Scuseria, M. A. Robb, J. R. Cheeseman, G. Scalmani, V. Barone, G. A. Petersson, H. Nakatsuji, X. Li, M. Caricato, A. Marenich, J. Bloino, B. G. Janesko, R. Gomperts, B. Mennucci, H. P. Hratchian, J. V. Ortiz, A. F. Izmaylov, J. L. Sonnenberg, D. Williams-Young, F. Ding, F. Lipparini, F. Egidi, J. Goings, B. Peng, A. Petrone, T. Henderson, D. Ranasinghe, V. G. Zakrzewski, J. Gao, N. Rega, G. Zheng, W. Liang, M. Hada, M. Ehara, K. Toyota, R. Fukuda, J. Hasegawa, M. Ishida, T. Nakajima, Y. Honda, O. Kitao, H. Nakai, T. Vreven, K. Throssell, J. A. Montgomery, Jr., J. E. Peralta, F. Ogliaro, M. Bearpark, J. J. Heyd, E. Brothers, K. N. Kudin, V. N. Staroverov, T. Keith, R. Kobayashi, J. Normand, K. Raghavachari, A. Rendell, J. C. Burant, S. S. Iyengar, J. Tomasi, M. Cossi, J. M. Millam, M. Klene, C. Adamo, R. Cammi, J. W. Ochterski, R. L. Martin, K. Morokuma, O. Farkas, J. B. Foresman, and D. J. Fox, Gaussian, Inc., Wallingford CT, 2016.

(65) Yanai, T.; Tew, D. P.; Handy, N. C. A New Hybrid Exchange-Correlation Functional Using the Coulomb-Attenuating Method (Cam-B3lyp). *Chem Phys Lett* **2004**, *393*, 51.

(66) Zaho, Y.; Truhlar, D. G. The M06 Suite of Density Functionals for Main Group Thermochemistry, Thermochemical Kinetics, Noncovalent Interactions, Excited States, and

1  
2  
3 Transition Elements: Two New Functionals and Systematic Testing of Four M06-Class  
4 Functionals and 12 Other Functionals. *Theor. Chem. Acc.* **2007**, *120*, 215.

5 (67) Martyniak, A.; Majerz, I.; Filarowski, A. Peculiarities of Quasi-Aromatic Hydrogen  
6 Bonding. *RSC Adv.* **2012**, *2*, 8135.

7 (68) Masumian, E.; Nowroozi, A. Computational Investigation on the Intramolecular  
8 Resonance-Inhibited Hydrogen Bonding: A New Type of Interaction Versus the Rahb Model.  
9 *Theor. Chem. Acc.* **2015**, *134*.

10 (69) Lin, X. H.; Zhang, H. Y.; Jiang, X.; Wu, W.; Mo, Y. R. The Origin of the Non-  
11 Additivity in Resonance-Assisted Hydrogen Bond Systems. *J. Phys. Chem. A.*, **2017**, *121*, 8535.

12 (70) Clark, S.; Segall, M. D.; Pickard, C. J.; Hasnip, P. J.; Probert, M. J.; Refson, K.;  
13 Payne, M. C. Z. *Krystallogr.* **2005**, *220*, 567.

14 (71) Perdew, J. P.; Burke, K.; Ernzerhof, M. Generalized Gradient Approximation  
15 Made Simple. *Phys. Rev. Lett.* **1996**, *77*, 3865.

16 (72) Tkatchenko, A.; Scheffler, M. Accurate Molecular Van Der Waals Interactions  
17 from Ground-State Electron Density and Free-Atom Reference Data. *Phys. Rev. Lett.* **2009**, *102*.

18 (73) Xia, S. H.; Gan, L.; Wang, K. H.; Li, Z.; Ma, D. W. Copper-Catalyzed Hydroxylation  
19 of (Hetero)Aryl Halides under Mild Conditions. *J. Am. Chem. Soc.* **2016**, *138*, 13493.